Mauren Abreu de Souza
Humberto Remigio Gamba
Helio Pedrini *Editors*

Multi-Modality Imaging

Applications and Computational Techniques

Springer

Multi-Modality Imaging

Mauren Abreu de Souza
Humberto Remigio Gamba • Helio Pedrini
Editors

Multi-Modality Imaging

Applications and Computational Techniques

Springer

Editors
Mauren Abreu de Souza
Graduate Program on Health Technology (PPGTS)
Pontifical Catholic University of Paraná – PUCPR
Curitiba, Paraná, Brazil

Humberto Remigio Gamba
Federal University of Technology – Paraná (UTFPR)
Curitiba, Paraná, Brazil

Helio Pedrini
Institute of Computing
University of Campinas
Campinas, SP, Brazil

ISBN 978-3-319-98973-0 ISBN 978-3-319-98974-7 (eBook)
https://doi.org/10.1007/978-3-319-98974-7

Library of Congress Control Number: 2018960266

This Springer imprint is published by the registered company Springer Nature Switzerland AG
The registered company address is: Gewerbestrasse 11, 6330 Cham, Switzerland

Preface

This book presents different approaches on multimodality imaging with a focus on biomedical applications. In terms of medical imaging, it is possible to divide into two categories: functional (related to physiological body measurements) and anatomical (structural) imaging modalities.

It is worth mentioning that this book covers some imaging combination coming from the usual popular modalities (such as the anatomical modalities, e.g. X-ray, CT and MRI); but it also includes some promising and new imaging modalities that are still being developed and improved (such as infrared thermography (IRT) and photoplethysmography imaging (PPGI)), implying in potential approaches for innovative biomedical applications.

Moreover, it includes a variety of tools on computer vision, imaging processing and computer graphics, which led to the generation and visualization of 3D models, allowing the most recent advances in this area possible. This is an ideal book for students and biomedical engineering researchers covering the biomedical imaging field.

The book covers a wide range of topics employing different multimodality imaging techniques for biomedical applications. The book is distributed in nine chapters, as follows:

Chapter 1—Infrared Thermography
Regarding non-invasive and non-contact imaging modalities, **infrared thermography (IRT)** is presented in the first chapter. Such modality is also called infrared (IR) imaging or thermal imaging. The main approach here is related to the diagnosis of several diseases, including breast cancer, rheumatic diseases, vascular diseases, etc. Apart from the diagnostic approach, the constant monitoring is also increasing its relevance in a wide range of different medical fields (i.e. the acquisition of vital signs, including temperature, respiratory rate, heart rate and blood perfusion). A recent approach still to be further explored involves the expansion towards 3D infrared imaging applications.

Chapter 2—Photoplethysmography Imaging and Common Optical Hybrid Imaging Modalities
Still presenting non-invasive and contactless approaches, the second chapter allows obtaining skin perfusion studies. In such modality, the active photoplethysmography imaging (PPGI) provides the mapping of dermal blood perfusion dynamics. The definition of PPGI consists in a classical photoplethysmography and pulse oximetry (SpO_2), which actually involves the remote opto-electronical measurement of arterial and/or venous blood volume changes. Although the results presented are very promising, they are still preliminary, since they still need to be standardized as a clinical application, especially for removing movement artefacts.

Chapter 3—Multimodal Image Fusion for Cardiac Resynchronization Therapy Planning
Cardiac resynchronization therapy (CRT) is due to treat patients with left-sided heart failure. This chapter presents optimizations of preoperative CRT plan, in order to produce increasing rates of such therapies. They had used a variety of imaging modalities, describing the anatomy, mechanical activation and tissue characteristics of the left ventricular (LV) under study. The authors developed a full workflow to process, register and fuse computer tomography (CT) images, ultrasound (US) images and magnetic resonance imaging (MRI). The results are represented as 3D patient-specific models, describing the anatomy of the involved heart regions (such as the LV, the coronary veins), even the electromechanical delays and the presence of fibrosis. The results obtained with such 3D patient-specific models are helping physicians to select the best surgical procedures, involving the most adequate LV pacing sites.

Chapter 4—CFD-Based Postprocessing of CT-MRI Data to Determine the Mechanics of Rupture in Abdominal Aortic Aneurysms
An approach employing a combination of two different imaging modalities (CT and MRI) for an application involving computational fluid dynamics (CFD) is presented in this chapter. The application involves a case study of diagnosis and surgical intervention's decision on abdominal aortic aneurysms (AAA). In the presented study, since the clinical metric is not enough for the prognoses rupture, a mechanics-based approach and computational fluid dynamics (CFD) are also undertaken. This is important since a patient-specific geometry and boundary conditions are employed for the analysis. In addition, a fluid structure interaction (FSI)-based analysis of the abnormal aorta is employed. An important conclusion is outlined in this study that the maximum transverse diameter is not the only parameter of AAA rupture's risk. Additionally, the mechanics approach based on multimodality image methodology produced a better diagnosis.

Chapter 5—Human Head Modelling Simulation Applied to Electroconvulsive Therapy
Regarding the generation of 3D realistic human head models, this chapter reconstructed such models based on magnetic resonance images. The problematic here is because it is aimed for electroconvulsive therapy (ECT) applications for treating

neurological conditions, once ECT uses low frequency and high amplitude of current, during a short period of time. Then, such electrical stimulation may generate heat due to the Joule effect. So, bio-heat transfer equation and Laplace equation were implemented for computational investigation. The results were analysed based on two points of view: thermal conductivity (which proved to be brain's safe) and electrical conductivity (which is an important factor to be taken into account).

Chapter 6—Use of Photon Scattering Interactions in Diagnosis and Treatment of Diseases

Regarding the use of invasive imaging modalities, such as photon scattering applications in medicine, it presented two types of scattering events: incoherent (Compton) and coherent (Rayleigh). Therefore, first this chapter presents an overview of Compton cameras for gamma imaging, in the context of proton beam therapy. Potential methods for in vivo proton range verification are also presented. Additionally, the principle of operation of the Compton cameras and imaging reconstruction techniques is included (i.e. back-projection and stochastic approaches). Later, the chapter presents tissue diffraction, which is based on coherent scattering as a diagnostic tool. X-ray diffraction (XRD) is presented in order to help in the differentiation of both health and cancerous tissue, based on the ability to discriminate tissue types. Further, some results including the generation of surface-rendered 3D volumes are presented, in order to allow the 3D differentiation of the tissues investigated (between tumour and normal tissue).

Chapter 7—Digital Breast Tomosynthesis: Systems, Characterization and Simulation

This chapter also focuses on invasive imaging modalities. Digital breast tomosynthesis (DBT) is an imaging application for breast cancer detection, which allows the generation of quasi-3D reconstruction images. First, this chapter presents an introduction and extensive review about digital X-ray tomosynthesis, including details about geometries, performance of the detectors, automatic exposure control performance, response function noise analysis, modulation transfer function (MTF), etc. Then, the image quality measurements are presented, since these issues are important for clinical tasks, such as the detection of microcalcifications. The last part of this chapter covers image simulation methods for DBT optimization. Several aspects are considered (e.g. image acquisition parameters, detector response, system geometry, radiation dose and image processing and reconstruction algorithms) considering acceptable breast doses as well. Regarding the clinical trials, there are two approaches, either involving a huge group of volunteers (asymptomatic women) or based on image simulation methods (virtual trials). The last option consists in fast, radiation-free and cost-effective option.

Chapter 8—Out-of-Core Rendering of Large Volumetric Data Sets at Multiple Levels of Detail

Regarding the massive high-resolution volume data (especially obtained from the anatomical imaging modalities, such as X-ray, microtomography, ultrasonography and magnetic resonance imaging), there is a constant need for being able to

computationally deal with all these data. Then, the traditional in-core volume rendering is quite limited. So, this chapter presents an architecture for out-of-core volume rendering, keeping the levels of detail. Therefore, several experiments were conducted in order to show the improvements of such approach, especially in terms of memory storage, computational required time during the rendering process and even frame rate.

Chapter 9—Geometric and Topological Modelling of Organs and Vascular Structures from CT Data

Still related to the generation and visualization of 3D models, the automatic segmentation of computer tomography (CT) images is a topic of interest. So, this chapter deals with the several modelling problems, mainly for surgery planning and training applications. For example, some of the issues presented are transformation and extraction of DICOM data, organs with branching or complex structures, polygon triangulation and file formats, among other issues. In general, the proposed solutions are related to allow the algorithms to be used together in order to provide surface-based reconstructions not only of organs but also at vascular structures, which can even be visualized with transparency.

The common approach among all these chapters is that either they employ the combination of functional and/or anatomical imaging, leading to multimodality imaging, or they apply different imaging modalities in order to generate 3D imaging data. The promising biomedical applications presented here are (1) the acquisition of vital signs from infrared thermography images (including temperature, respiratory rate, heart rate and blood perfusion), (2) dermal blood perfusion dynamics (involving photoplethysmography and optical hybrid imaging modalities), (3) 3D generation of abdominal aortic aneurysms (AAA) (including computational fluid dynamics (CFD), fluid structure interaction (FSI) and mechanical approaches), (4) cardiac resynchronization therapy (CRT) involving the 3D generation of not only the heart but also specific regions of it (e.g. left ventricular (LV) and coronary veins) and (5) the generation of 3D realistic human head models (from MRI data) for electroconvulsive therapy applications; regarding the use of invasive radiation, such as (6) X-ray diffraction (XRD) for 3D differentiation between tumour and normal tissues and (7) digital breast tomosynthesis (DBT) for the generation of quasi-3D reconstruction of the breast, for cancer detection; and finally, some of the computational techniques that are allowing all these lately improvements, for example, (8) dealing with the out-of-core volume rendering of all the massive high resolution volume data involving medical imaging and (9) the generation and visualization of 3D models mainly for surgery planning and training applications.

Curitiba, Paraná, Brazil — Mauren Abreu de Souza
Curitiba, Paraná, Brazil — Humberto Remigio Gamba
Campinas, SP, Brazil — Helio Pedrini

Contents

Contributors

Tony Ahfock University of Southern Queensland, Darling Heights, QLD, Australia

Amany Amin John Radcliffe Hospital, Oxford, UK

St Bartholomew's Hospital, London, UK

Paulo Henrique Junqueira Amorim Division of 3D Technologies, Center for Information Technology Renato Archer, Campinas, SP, Brazil

Carina Barbosa Pereira Chair for Medical Information Technology, Helmholtz-Institute for Biomedical Engineering, RWTH Aachen University, Aachen, Germany

Julian Betancur Univ Rennes, CHU Rennes, Inserm, LTSI – UMR 1099, Rennes, France

Université de Rennes 1, LTSI, Rennes, France

Nikolai Blanik Chair for Medical Information Technology, Helmholtz-Institute for Biomedical Engineering, RWTH Aachen University, Aachen, Germany

Claudia Rosa Blazek The Private Clinic of Dermatology, Haut im Zentrum, Zurich, Switzerland

Vladimir Blazek Chair for Medical Information Technology, Helmholtz-Institute for Biomedical Engineering, RWTH Aachen University, Aachen, Germany

Czech Institute of Informatics, Robotics and Cybernetics (CIIRC), Czech Technical University in Prague, Prague, Czech Republic

Sophie Bruge Univ Rennes, CHU Rennes, Inserm, LTSI – UMR 1099, Rennes, France

Université de Rennes 1, LTSI, Rennes, France

Tejas Canchi School of Mechanical and Aerospace Engineering, Nanyang Technological University, Singapore, Singapore

Hugo Capote Hospital Dr. José Maria Grande, Portalegre, Portugal

Nicolas Courtial Univ Rennes, CHU Rennes, Inserm, LTSI – UMR 1099, Rennes, France

Université de Rennes 1, LTSI, Rennes, France

Chiaki Crews Department of Medical Physics & Biomedical Engineering, University College London, London, UK

Stephan Dahlmanns Chair for Medical Information Technology, Helmholtz-Institute for Biomedical Engineering, RWTH Aachen University, Aachen, Germany

Erwan Donal Univ Rennes, CHU Rennes, Inserm, LTSI – UMR 1099, Rennes, France

Université de Rennes 1, LTSI, Rennes, France

Mireille Garreau Univ Rennes, CHU Rennes, Inserm, LTSI – UMR 1099, Rennes, France

Université de Rennes 1, LTSI, Rennes, France

Andrea Gutierrez Department of Medical Physics & Biomedical Engineering, University College London, London, UK

Andria Hadjipanteli Medical School, University of Cyprus, Nicosia, Cyprus

Alfredo Hernandez Univ Rennes, CHU Rennes, Inserm, LTSI – UMR 1099, Rennes, France

Université de Rennes 1, LTSI, Rennes, France

Francesco Iacoviello Electrochemical Innovation Lab, Department of Chemical Engineering, University College London, London, UK

Selina Kolokytha Empa, Centre for X-Ray Analytics, Swiss Federal Laboratories for Materials Science and Technology, Dübendorf, Switzerland

Anastasios Konstantinidis Diagnostic Radiology and Radiation Protection Service, Christie Medical Physics and Engineering, The Christie NHS Foundation Trust, Manchester, UK

Christophe Leclercq Univ Rennes, CHU Rennes, Inserm, LTSI – UMR 1099, Rennes, France

Université de Rennes 1, LTSI, Rennes, France

Mathieu Lederlin Univ Rennes, CHU Rennes, Inserm, LTSI – UMR 1099, Rennes, France

Université de Rennes 1, LTSI, Rennes, France

Steffen Leonhardt Chair for Medical Information Technology, Helmholtz-Institute for Biomedical Engineering, RWTH Aachen University, Aachen, Germany

Yan Li University of Southern Queensland, Darling Heights, QLD, Australia

Marília Menezes de Oliveira The University of Sydney, Sydney, NSW, Australia

University of Southern Queensland, Darling Heights, QLD, Australia

Thiago Franco de Moraes Division of 3D Technologies, Center for Information Technology Renato Archer, Campinas, SP, Brazil

Robert Moss Department of Medical Physics & Biomedical Engineering, University College London, London, UK

José Luis Moyano-Cuevas Bioengineering and Health Technology Unit, Jesús Usón Minimally Invasive Surgery Center, Cáceres, Spain

Sriram Narayanan Department of General Surgery, Tan Tock Seng Hospital, Singapore, Singapore

Eddie Y. K. Ng School of Mechanical and Aerospace Engineering, Nanyang Technological University, Singapore, Singapore

João Fradinho Oliveira C3i + CIAUD, Instituto Politécnico de Portalegre + Universidade de Lisboa, Lisboa, Portugal

José Blas Pagador Bioengineering and Health Technology Unit, Jesús Usón Minimally Invasive Surgery Center, Cáceres, Spain

Helio Pedrini Institute of Computing, University of Campinas, Campinas, SP, Brazil

Francisco Miguel Sánchez-Margallo Jesús Usón Minimally Invasive Surgery Center, Cáceres, Spain

Ashish Saxena School of Mechanical and Aerospace Engineering, Nanyang Technological University, Singapore, Singapore

Paul Shearing Electrochemical Innovation Lab, Department of Chemical Engineering, University College London, London, UK

Jorge Vicente Lopes da Silva Division of 3D Technologies, Center for Information Technology Renato Archer, Campinas, SP, Brazil

Antoine Simon Univ Rennes, CHU Rennes, Inserm, LTSI - UMR 1099, Rennes, France

Université de Rennes 1, LTSI, Rennes, France

Bo Song University of Southern Queensland, Darling Heights, QLD, Australia

Robert Speller Department of Medical Physics & Biomedical Engineering, University College London, London, UK

François Tavard Univ Rennes, CHU Rennes, Inserm, LTSI - UMR 1099, Rennes, France

Université de Rennes 1, LTSI, Rennes, France

Daniel Teichmann Chair for Medical Information Technology, Helmholtz-Institute for Biomedical Engineering, RWTH Aachen University, Aachen, Germany

Sarah Vinnicombe The Breast Unit, Cheltenham, Gloucestershire Hospitals NHS Foundation Trust, Gloucester, UK

The University of Dundee, Dundee, UK

Paul Wen University of Southern Queensland, Darling Heights, QLD, Australia

Xinchi Yu Chair for Medical Information Technology, Helmholtz-Institute for Biomedical Engineering, RWTH Aachen University, Aachen, Germany

Chapter 1
Infrared Thermography

Carina Barbosa Pereira, Xinchi Yu, Stephan Dahlmanns, Vladimir Blazek, Steffen Leonhardt, and Daniel Teichmann

Abstract Infrared thermography (also infrared imaging or thermal imaging) is a new remote, non-contact and non-invasive diagnostic and monitoring technique with increasing relevance in a wide range of medical fields. This is mainly due to the several advantages of this technology. Thermal imaging is a passive technique which detects the radiation naturally emitted from an object, in this case the human skin, and does not use any harmful radiation. Thus, infrared thermography (IRT) is suitable for prolonged and repeated use. In the last decades, new medical applications for thermal imaging have arisen. These techniques have been successfully used in the diagnosis of several pathologies, including breast cancer, rheumatic diseases, dry eye syndrome, vascular diseases, etc. Infrared thermography has also demonstrated its potential in the monitoring of several vital signs, including temperature, respiratory rate, heart rate, and blood perfusion. Recently, there has been new advance in 3D infrared imaging. A three-dimensional thermal signature may provide several advantages in the detection and monitoring of the course of several pathologies including arthritis, thyroid dysfunctions, breast cancer, sports lesions, and diabetic foot. The current chapter focuses on advances in the area of medical IRT. First, it reviews the basics of IRT and essential theoretical background. Second, some medical applications and corresponding methods are

Carina Barbosa Pereira, Xinchi Yu, and Stephan Dahlmanns contributed equally to this work.

C. Barbosa Pereira (✉) · X. Yu · S. Dahlmanns · S. Leonhardt · D. Teichmann
Chair for Medical Information Technology, Helmholtz-Institute for Biomedical Engineering, RWTH Aachen University, Aachen, Germany
e-mail: pereira@hia.rwth-aachen.de

V. Blazek
Chair for Medical Information Technology, Helmholtz-Institute for Biomedical Engineering, RWTH Aachen University, Aachen, Germany

Czech Institute of Informatics, Robotics and Cybernetics (CIIRC), Czech Technical University in Prague, Prague, Czech Republic

M. Abreu de Souza et al. (eds.), *Multi-Modality Imaging*,
https://doi.org/10.1007/978-3-319-98974-7_1

described in detail. Third, it gives an overview on the recent advances on "3D Infrared Thermography".

Keywords Infrared thermography · Medical applications · Diagnostic · Monitoring · 3D infrared thermography

1.1 Introduction

Infrared thermography (IRT), also known as thermal imaging, is an imaging modality, which senses infrared radiation (heat) emitted by objects. In contrast to other imaging techniques in medicine, such as X-Ray, computed tomography (CT), and magnetic resonance imaging (MRI), IRT is a completely passive—i.e., non-invasive and non-radiating—measurement technique. The first infrared thermogram of a human was recorded in 1928 by Prof. Czerny in Frankfurt, Germany [1]. Initially, only single infrared detectors have been used. Later on, during World War II, infrared detectors have been developed and used for military applications [2]. Besides the issues regarding availability (military restrictions) and price, that technology was unsuitable for medical applications: both thermal resolution (approx. 0.5 K) and spatial resolution (approx. 5 mm at a target size of 50 cm^2) were too low in order to detect small temperature differences and anatomic structures on the human body. Moreover, the infrared detectors were big and needed cooling by, e.g., nitrogen, argon gas, or a sterling cooler [3]. It was only in the 1990s and early 2000s when the development and availability of uncooled microbolometer focal plane arrays (FPA) pioneered the usage of IRT in medicine. In contrast to the old devices with single detectors, the new cameras with FPAs provided a high spatial and thermal resolution. Also temporal resolution (sample rate or scanning speed) increased, enabling real-time and high-speed recordings. Another factor was the availability of computers and more user-friendly image processing software [3, 4].

A widely known medical application of modern IRT is mass fever screening during worldwide pandemics, for example, at airports. With the general trend in medicine away from a reactive, curative approach (diagnosis and treatment) towards a proactive and preventive approach (identification of risks and elimination of those), IRT is playing an important role. Since it can easily detect anomalies of body surface temperature, i.e., hyperthermia due to inflammation or hypothermia induced by poor perfusion, there are multiple medical applications [4]. In this chapter, we will introduce some of them—detection of breast cancer, diagnosis of rheumatic diseases, dry eye syndrome, wounds, monitoring of vital sings (respiratory rate, cardiac pulse, and perfusion) as well as the capabilities of 3D thermal imaging.

1.2 Physical Principles of Infrared Thermography

Thermographic cameras are unable to sense the surface temperature of an object directly. Rather, the power of electromagnetic rays that hit the sensors of the cameras is measured. In this section the physical principles for the calculation of the surface temperature from its radiation are introduced. Additionally, the effects of non-ideal objects as well as effects of the transport medium in medical applications of thermographic measurements will be considered.

1.2.1 Thermal Radiation

All objects with a surface temperature above absolute zero (0 K or −273.15 °C, respectively) emit electromagnetic radiation with a particular wavelength (λ). This phenomenon is different from heat transfer due to the collusion of particles, called conduction, where the energy transport depends on the temperature gradient inside the transport medium. Radiation, on the other hand, describes the energy transfer by electromagnetic waves, which is solely dependent on the temperature of the radiation source. For example, the electromagnetic radiation of the sun reaches Earth even though the temperature of outer space is constant.

The theory of radiant heat was first described by Max Planck in 1913 and is the fundamental basis of the calculation of surface temperatures based on the spectral analysis of its radiation [5].

1.2.2 Blackbody Radiation

A practical way to describe the energy flux of radiation is via an idealized physical body called "blackbody". A blackbody absorbs all incident radiant energy without reflection and is homogeneous as well as isotropic. Hence, its radiation is emitted uniformly in all directions of space. In addition, it is postulated that all radiation of a blackbody is entirely dependent on the body's absolute temperature, therefore the phenomena of luminescence are excluded from calculations. In order to describe thermal radiation, the permanent state will be investigated, which means that the energy and thus the temperature of the blackbody are distributed equally inside its volume.

Based on these assumptions, it is possible to calculate the spectral distribution of thermal radiation emitted by a blackbody. This function was first described by Max Planck as the Planck spectrum M_λ^0 and follows the equation:

$$M_\lambda^0(\lambda, T) = \frac{2\pi hc^2}{\lambda^5 \cdot (e^{\frac{hc}{\lambda kT}} - 1)}. \tag{1.1}$$

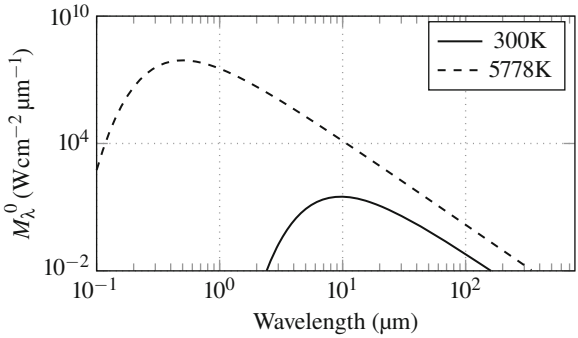

Fig. 1.1 Spectral radiant exitance of a body (M_λ^0) at two different temperatures: 300 and 5778 K (surface temperature of the sun)

Here, M_λ^0 represents the spectral radiant exitance of the blackbody in (W m^{-2} µm^{-1}), λ is the wavelength (µm), T stands for the surface temperature (K), h denotes the Planck constant ($h = 6.626 \times 10^{-34}$ J s), $k = 1.3807 \times 10^{-23}$ J K^{-1} corresponds to the Boltzmann constant, and $c = 2.998 \times 10^{8}$ m s^{-1} is the speed of light in vacuum. M_λ^0 is a function of λ, which means that the total energy content is distributed over a range of wavelengths. This resulting energy distribution is dependent on the temperature T of the blackbody as displayed in Fig. 1.1.

The shape of the Planck spectrum is similar for all temperatures, but its amount of power as well as the wavelength of maximum power (λ_{max}) is shifted based on the surface temperature. For example, the surface temperature of the sun equals 5778 K; this creates a spectrum with a wavelength of maximum power at around $\lambda_{max} \approx$ 500 nm (the wavelength where human eyes evolved to be most sensitive ranges between about 390 and 700 nm). Bodies with surface temperatures around 300 K (26.85 °C) generate a Planck spectrum between 2.5 and 150 µm. As temperature decreases, the radiation emitted is more in the range of longer wavelengths. This effect is explained by Wien's displacement law. Wavelengths created by surface temperatures of around 300 K are invisible for the human eye, but sensors that are sensitive around 10 µm are able to detect this radiation, just like human eyes can detect the radiation emitted by the sun [6].

Surface temperatures can be calculated based on the total radiant power per surface area M (W m^{-2}). Hence, it is not necessary for thermal detectors to distinguish between different wavelengths. In general, M describes the area underneath the curves given in Fig. 1.1; it can be calculated by integrating M_λ^0 over the range of all significant wavelengths as given by

$$M = \int_{\lambda^0=0}^{\infty} M_\lambda^0 \, \mathrm{d}\lambda. \tag{1.2}$$

The solution of the integral can be estimated by applying the Stefan-Boltzmann law:

$$M = \sigma \cdot T^4, \tag{1.3}$$

where $\sigma = 5.67 \times 10^{-8}$ W m^{-2} K^{-4} is the Stefan-Boltzmann constant. With this equation the surface temperature of an object can be easily calculated based on the

measurement of the radiated power per surface area. This is the general working principle of sensors integrated in thermographic cameras.

1.2.3 Greybody Radiation

Both Planck's and Stefan-Boltzmann's law describe the radiation of a blackbody under ideal conditions. Nevertheless, real bodies often do not absorb all radiant energy. In general, objects interact in three different ways with radiation: by absorption (α), reflection (β), and transmission (γ). Considering the law of conservation of energy, $\alpha + \beta + \gamma = 1$ applies. For black bodies, the absorption value α equals 1 and reflection and transmission are zero. If the absorption value is less than 1, the considered object is called a "greybody". Solid bodies are generally opaque (transmission $\gamma = 0$), and consequently $\alpha + \beta = 1$.

According to Kirchhoff's law, at a given temperature the ratio of radiant absorbance to emittance is constant for greybodies ($\alpha = \epsilon$), therefore the emissivity for each wavelength is described by

$$\epsilon = 1 - \beta_\lambda. \tag{1.4}$$

For greybodies the Stefan-Boltzmann law takes the form

$$M = \epsilon \cdot \sigma \cdot T^4, \tag{1.5}$$

where ϵ is constant for all wavelengths. Since ϵ is smaller than 1 for greybodies, their temperature has to be larger to create the same total radiant power of blackbodies.

1.2.4 Temperature Measurement

As mentioned previously, thermal cameras measure and convert the radiation energy emitted by a body into a temperature value. However, not all radiation detected by the camera sensors corresponds to the target object. The measured energy (W_{tot}) rather consists of the emission of the object (E_{obj}) plus reflected emission from ambient sources (E_{amb}) and emission from the atmosphere (E_{atm}).

The atmosphere describes the transport medium of heat radiation. In this medium, there are molecules that interact with the heat rays: some of its energy gets absorbed or scattered and the atmospheric transmittance γ_{atm} must be considered. Therefore, the Stefan-Boltzmann law for black bodies in vacuum,

$$M_{\text{measured}} = \sigma \cdot T_{\text{obj}}^4, \tag{1.6}$$

Table 1.1 Parameters used to calculate the temperature of the target object T_{obj}

Parameter	Symbol	Value
Total radiant power	M_{measured}	Measured by the camera
Emittance of object	ϵ_{obj}	Unknown/estimated
Transmittance of atmosphere	γ_{atm}	Approximated: $\gamma_{\text{atm}} \cong 1$
Stefan-Boltzmann constant	σ	$5.67 \times 10^{-8}\,\text{W}\,\text{m}^{-2}\,\text{K}^{-4}$
Temperature of ambient objects	T_{amb}	Unknown
Temperature of the atmosphere	T_{atm}	Unknown

must be adapted for greybodies in the atmosphere:

$$M_{\text{measured}} = \epsilon_{\text{obj}} \cdot \gamma_{\text{atm}} \cdot \sigma \cdot T_{\text{obj}}^4 + (1-\epsilon_{\text{obj}}) \cdot \gamma_{\text{atm}} \cdot \sigma \cdot T_{\text{amb}}^4 + (1-\gamma_{\text{atm}}) \cdot \sigma \cdot T_{\text{atm}}^4. \quad (1.7)$$

The parameters necessary to compute the temperature of the target object T_{obj} are displayed in Table 1.1. Next to the Stefan-Boltzmann constant σ and the measured radiation M_{measured}, additional information about the object itself (namely, object's emittance ϵ_{obj}) and its environment (such as temperature of the atmosphere T_{atm}, temperature of ambient objects T_{amb}, and transmittance of the atmosphere γ_{atm}) need to be known.

The transmittance of a medium can vary very strongly for different wavelengths. For example, visible light propagates through water with few losses (you can see very far in clear water) in contrast to infrared light that is completely absorbed by the water molecules. The transmittance for wavelengths above 1500 nm approximates zero. This makes impossible the use of IRT under water. The transmittance of air γ_{atm} is dependent on the wavelength as well. As opposed to water, there exists a transmittance window that makes thermography possible. For a significant range of wavelengths, γ_{atm} is approximately 1. Thus, when air is the transport medium, Eq. (1.7) can be further simplified

$$M_{\text{measured}} \cong \epsilon_{\text{obj}} \cdot \sigma \cdot T_{\text{obj}}^4 + (1 - \epsilon_{\text{obj}}) \cdot \sigma \cdot T_{\text{amb}}^4. \quad (1.8)$$

Now, the relation between measured power and the object's temperature is independent from air temperature.

There are many sources of thermal radiation that could increase the thermal radiation without increasing the object's temperature, for example, the sun, heating or light bulbs, especially when the emissivity of the greybody is noticeably below 1. In practice, the operator of a thermal camera should make sure that there are no ambient heat radiation sources close to the object of interest. In this case the equation further simplifies to

$$M_{\text{measured}} \cong \epsilon_{\text{obj}}. \quad (1.9)$$

Finally, in order to correctly calculate a surface temperature based on the radiation, the emissivity ϵ_{obj} of the object needs to be known. Many thermal cameras give the option to input the emissivity value of the object that is currently measured. However, this value is often unknown or multiple objects with different emissivity values are measured at the same time. The consequences are systematic measurement errors that distort the results, i.e., the output of the camera.

In medical applications, the surface area of interest often consists of human skin. Its emissivity ϵ_{skin} is well known, approximately 0.97–0.99 for temperatures around 300 K. Therefore, blackbody theory can be applied for the measurement of skin surface temperatures. In contrast, the emissivity of inner organs like the heart is noticeably below 1. This has to be considered for surgical applications of thermal imaging [7, 8].

1.2.5 Thermal Cameras

There are multiple types of thermal detectors capable of converting infrared radiation into electrical signals. For medical applications, these systems need to be saved, easy to use, and inexpensive. Traditionally, thermographic cameras have been used for maintenance and research especially in industrial processes, like engine diagnostics or power electronics. These cameras are capable of covering a thermal range from values below 0 °C up to temperatures far above 1000 °C and use detectors that often require active cooling. Additionally, the lenses of most thermal cameras cannot to be made of glass whose transmissivity approaches zero for wavelengths above 4500 nm. Hence, rare materials such as Germanium or sapphire crystals need to be incorporated.

Cameras for standard clinical applications use sensors that cover the wavelength spectrum from 3 to 5 µm (mid-wave infrared) and from 7 to 14 µm (long wave infrared), and therefore the bulk of the Planck spectrum of human skin temperatures (around 300 K). They reach temporal resolutions of 30 frames per second (fps) and make the analysis of dynamic temperature changes possible.

Thermographic cameras do not reach the spatial resolution of modern cameras in the visible spectrum, primarily because the sensor technology, active cooling, and materials for lenses are very expensive. High sensitivity hand-held infrared cameras reach resolutions of 2048 × 1536 pixels. Today, there are standard thermographic cameras on the market that do not require cooling and reach resolutions of 1024 × 768 pixels. Those camera types are often used for medical applications that will be further described in Sect. 1.3. Cameras for standard clinical applications use modern sensor technologies like microbolometer disposed on FPAs. These technologies reach thermal sensitivities below 0.1 °C, and their accuracy lies around 1 °C. They enable the analysis of small temperature changes on the surface of an object, like the temperature distribution on the human skin [9]. Nevertheless, the thermal accuracy of infrared cameras does not allow for sophisticated diagnostics of absolute temperatures, especially when the effects of unknown emissivities (as described above) are taken into account [10, 11].

1.3 Medical Applications

In the last decades several medical applications for thermal imaging cameras started to emerge. The next sections present some of the current applications of IRT for both medical fields, diagnosis and monitoring.

1.3.1 Diagnosis

A healthy human body presents a symmetric temperature distribution around the sagittal plane [12]. However, there are several biological factors that might influence the human body temperature, locally or systemically. Therefore, any deviation from normal can be an indicator of pathophysiologic anomalies, such as inflammation, carcinogenesis, or neuropathology [13]. The first use of temperature for health assessment dates back to 400 BC in the writings of Hippocrates. Hippocrates routinely slathered wet mud and clay over the patients' bodies speculating that the areas where the mud dried first had a disease [14]. Abnormal thermal patterns can be easily recognized in thermal imaging. Therefore, an early diagnosis of certain diseases is possible through the analysis of thermograms. In the last couple of years, IRT has found a wide acceptance among the medical community due to its advantages. Thermal imaging is a remote, non-contact, non-invasive, and passive technique. It only records the natural radiation emanated from the skin surfaces and does not use any harmful radiation [2, 15]. Lastly, IRT is a real-time technology, enabling monitoring of dynamic variations of body temperature. Due to all these advantages, thermal imaging has been considered an effective alternative diagnosis tool [2]. It has been being used in a variety of medical applications, including fields such as neurology, oncology, orthopedics, and dermatology [16]. Table 1.2 describes some medical applications, relevant research studies, and the hardware used. In the following sections only four applications will be presented in detail.

1.3.1.1 Detection of Breast Abnormalities

According to the World Health Organization, 1.7 million breast cancer cases occurred in 2012 worldwide. It is the most frequent cancer in women in 150 countries (approximately 25% of all cancer cases) as well as the most common cause of cancer-related death. It was estimated that 522,000 women died from this cancer in 2012 worldwide [38]. Studies demonstrated that an early detection can lead to 85% survival chance while a late detection of breast cancer leads to only 10%. Therefore, it is very important for physicians to identify in due course potentially threatening malignant tumors for a successful treatment [2]. Mammography is the current gold standard to examine the human breast. However, this technique exhibits low sensitivity in young women and in women with a

Table 1.2 Medical applications of IRT (Ref.—references)

Application	Year	Authors [Ref.]	IRT system
Breast cancer	2011	Kontos et al. [17]	Meditherm Med2000™ Pro (Meditherm, Medical Monitoring Systems Pty Ltd., Beaufort, NC, USA)
	2011	Umadevi et al. [18]	Fluke Ti40FT (M/s Fluke Corp., Everett, Washington, USA) and Varioscan 3021 ST (InfraTec GmbH, Dresden, Germany)
Complex regional pain syndrome	2006	Niehof et al. [19]	ThermaCam SC2000 (FLIR, Danderyd, Sweden)
	2008	Gardiner et al. [20]	FLIR A40M (FLIR Systems Boston, MA, USA)
	2016	Cho et al. [21]	IRIS-5000 (Medicore Co., Seoul, Korea)
Diabetic neuropathic foot	2006	Bharara et al. [22]	Unknown
Dry eye syndrome	2010	Tan et al. [23]	VarioCAM, JENOPTIK Laser (Germany)
	2017	Matteoli et al. [24]	FLIR 320A (FLIR Systems, Oregon, USA)
Knee injuries	2010	Hildebrandt et al. [4]	TVS-500EX (NEC Avio Infrared Technologies, Tokyo, Japan)
Low back pain	2006	Zaproudina et al. [25]	IRTIS-2000 C (IRTIS Ltd, Moscow, Russia)
Osteoarthritis	1981	Ring et al. [26]	Unknown
	2004	Varju et al. [27]	Compix PC2000e (Compix, Lake Oswego, OR, USA)
	2010	Denoble et al. [28]	Meditherm Med2000™ Pro (Meditherm, Medical Monitoring Systems Pty Ltd., Beaufort, NC, USA)
Peripheral arterial disease	2009	Bagavathiappan et al. [29]	AGEMA Thermovision 550 system (Danderyd, Sweden)
	2011	Huang et al. [30]	Spectrum 9000-MB Series (United Integrated Service Co. Ltd, Taipei Hsien, Taiwan)
	2016	Staffa et al. [31]	FLIR B200 (Flir Systems, Danderyd, Sweden)
Raynaud's phenomena	2014	Lim et al. [32]	IRIS-XP® (Medicore, Seoul)
Rheumatoid arthritis	2015	Lasanen et al. [33]	FLIR A325 (FLIR Systems Inc., USA)
	2017	Lerkvaleekul et al. [34]	FLIR E60 (FLIR System Inc., USA)
Shoulder impingement syndrome	2007	Park et al. [35]	IRIS 5000 (Medicore, Seoul, Korea)
Wound assessment	2015	Dini et al. [36]	FLIR T620 Thermal Imager (FLIR Systems Boston, MA, USA)
	2017	Keenan et al. [37]	FLIR A325 (FLIR Systems Boston, MA, USA)

greater breast density. In addition, this technique requires breast compression during screening and exposes the patient to harmful radiation (X-rays usually around 30 kVp). Several studies have demonstrated that thermal imaging may be a potential adjunctive tool for detecting this kind of cancer [38]. Breast thermography was firstly introduced by Lawson in 1956 [39]. According to this author, one of the biological characteristics of malignant tumors is the increased rate of growth in comparison to that of the surrounding tissues. This leads to an accelerated local metabolism, which is supported by increased blood and lymphatic vascularity, and consequently to localized hot spots [2, 39]. Amalric et al. screened over a period of 10 years 61,000 women using thermography [40]. Their outstanding study showed that thermal imaging was the earliest marker of breast cancer in approximately 60% of the cases [40]. In addition to passive breast imaging, there are other procedures to enhance thermographic contrast of tumors. The first is based on cold stimulation. The blood vessels which supply the tumors are simply endothelial tubes devoid of a muscular layer. Thus, during cold stress (sympathetic stimulus) they fail to vasoconstrict and show instead a hyperthermic pattern due to vasodilation [2]. The second procedure is based on induced evaporation. Deng and Liu [41] demonstrated that this technique enhances the temperature contrast in case of tumors underneath the skin. In short, the authors sprayed water and 75% of ethanol solution (evaporant) before imaging acquisition. They conclude that this method permitted to improve diagnostic accuracy, particularly in the early stage of deeply embedded tumors [41].

In 2012, Boquete et al. proposed a novel approach capable of detecting high tumor risk areas [42]. It was based on independent component analysis. For validation purposes, they used the database of the *Ann Arbor thermography center* comprising eight case studies, where two out of eight were control cases. The thermograms had YCbCr 480 × 380 pixels format and followed a color code: lower temperatures were shown in blue and higher temperatures in yellow-red tones; the highest temperatures were displayed in white. While Fig. 1.2a shows a control case, Fig. 1.2b, c denotes two cases of ductal carcinoma. The proposed method corroborated that the hot spots in the thermogram of the breast indicate a potentially cancerous zone. It presented a sensitivity of 100% and specificity of 94.7%. The positive and negative predictive values were 83% and 100%, respectively [42].

1.3.1.2 Rheumatic Diseases

Rheumatic diseases are a group of over 150 systemic autoimmune diseases (e.g., rheumatic arthritis, osteoarthritis and autoimmune diseases, such as systemic lupus erythematosus, scleroderma, osteoporosis, back pain, gout, fibromyalgia, and tendonitis) which are characterized by inflammation affecting the connecting or supporting structures of the body, mostly joints, but also tendons, ligaments, bones, and muscles. Common symptoms of these diseases include swelling, pain, stiffness, and decreased range of motion. Rheumatic diseases are one of the leading causes of disability in the USA affecting more than 50 million people of all ages, genders, and races. By 2040, the number of adults in the USA is expected to increase to 78.4 million.

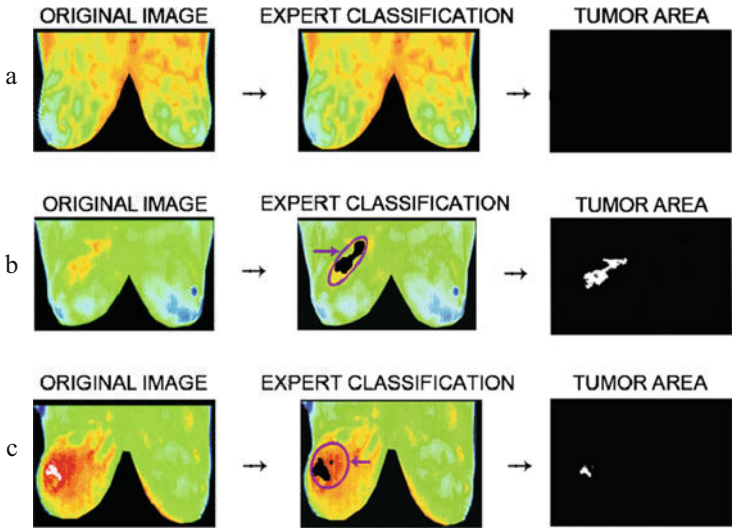

Fig. 1.2 (**a**) Control case. (**b**, **c**) Ductal carcinoma. Modified from Boquete et al. [42]

Currently, there are few tools for early diagnosis of rheumatic diseases and for assessing the effectiveness of therapies: bone scintigraphy, ultrasound, contrast enhanced ultrasound, magnetic resonance (MR), and contrast enhanced MR. However, these techniques are not readily available for the masses and waiting lists in many countries are very long. Therefore, less expensive technologies for diagnosis and therapy monitoring would be beneficial in this medical field.

IRT has been used in the diagnosis and assessment of recovery of some rheumatic diseases, including Raynaud's phenomena, gout, and arthritis [2]. In an outstanding publication, Ring [43] demonstrated that patients suffering from juvenile arthritis,[1] osteoarthrosis,[2] rheumatoid arthritis,[3] gout,[4] among others show abnormal temperature distributions over joints. To quantify joint inflammation, Collins et al. [44] developed in 1974 a "thermographic index":

[1]Juvenile arthritis, also known as pediatric rheumatic disease, is an umbrella term that describes autoimmune and inflammatory conditions or pediatric rheumatic diseases developed in children under the age of 16.

[2]Osteoarthrosis is the most frequent chronic condition of the joints, affecting more than 30 million Americans. It can affect any joint, but it occurs most commonly in knees, hips, lower back and neck, small joints of the fingers, among others.

[3]Rheumatoid arthritis is an autoimmune disease in which the body's immune system mistakenly attacks the joints.

[4]Gout is a form of inflammatory arthritis that affects people who have high levels of uric acid in the blood. Uric acid can form needle-like crystals in the joints. The most common symptoms are sudden and severe episodes of pain, tenderness, redness, warmth, and swelling.

$$\frac{\sum(\Delta t \times a)}{A}, \tag{1.10}$$

where Δt stands for the difference between the measured isothermal temperature and a constant (26 °C); a is the area occupied by isotherm (region of the thermogram with the same temperature); and A corresponds to the total area of the thermogram. In other study, Ring et al. [45] studied the ability of thermal imaging to detect and quantify the effects of non-steroidal anti-inflammatory drugs (such as aspirin, indomethacin, and benorylate) in patients with gout and rheumatoid arthritis [45]. The results indicated that IRT is a suitable tool for assessment of the response to the anti-inflammatory treatment; the administration of a local anti-inflammatory caused a fall in the thermographic index of the inflamed joint. Frize et al. used, in turn, IRT for diagnosis of rheumatoid arthritis [46]. The authors reported that metacarpophalangeal joints of the index, middle fingers, and knee are the best indicators of the presence and absence of this disease [46]. Lerkvaleekul et al. studied the capability of IRT to detect wrist arthritis in juvenile idiopathic arthritis patients [34]. Using the mean temperature and maximum temperature at the skin surface in the region of interest, moderate wrist joint arthritis could be differentiated from severe and inactive arthritis. In 2009, Wu et al. published a work where they claimed that local skin temperature near the coccyx region decreases significantly after therapy in patients suffering from coccygodynia (pain in the coccyx or tailbone area) [47]. In this case, thermal imaging has demonstrated to be an effective tool for the assessment of coccygeal pain intensity after treatment. In contrast, Park et al. used IRT for the assessment of shoulder impingement syndrome [35]. They prospectively evaluated 100 patients with unilateral impingement syndrome, and a control group of 30 subjects. In IRT findings, 73% of the patients presented abnormal thermal changes, 51% displayed hypothermia, and 22% had hyperthermia. The results confirmed that in the hypothermic group limitation of shoulder motion was significantly more prominent than in the other groups: hyperthermic and normal groups. Commonly, shoulder immobility induces a localized muscle atrophy, which in turn causes apoptosis of the muscle's cells. This phenomenon may lead to a decreased blood flow in this region, resulting in hypothermic patterns in the skin of the shoulder [35]. Vecchio and associates [48] corroborated in their papers the findings of Park et al. [35]. They stated that the most part of the subjects with unilateral frozen shoulder had anomalous skin temperature distribution [48].

1.3.1.3 Dry Eye Syndrome and Ocular Disease

Dry eye syndrome is a disturbance of the tear film caused by a lack of adequate tears. Tears can be described as a complex mixture of water, mucus, and fatty oils, which make the surface of the eyes smother and clear and protect them from infection. Therefore, dry eye syndrome may lead to eye inflammation, vision problems, as well as scarring on the surface of the corneas.

Nowadays, there are some methods for diagnosis of dry eye. Film breakup time and tear osmolarity give information about tear functionality but do not specify the causes of possible damage. The objective clinical examination of corneal fluorescein staining may help in the diagnosis but is very fastidious.

In recent decades, the diagnostic of dry eye syndrome and ocular diseases using infrared thermography has been analyzed. Studies have demonstrated that patients with dry eye disease have cooler ocular surfaces than those of asymptomatic normal subjects [24, 49]. In 2009, Tan and associates [23] published a review paper describing different methodologies for manual, semi-manual, and automatic measure of ocular surface temperature in IRT.

Additionally, thermal imaging can be used for diagnosis and assessment of the inflammatory state in patients with Graves' ophthalmopathy as described by Chang et al. [50]. Note that Graves' orbitopathy is an autoimmune inflammatory disorder of the orbit and periorbital tissues. It is characterized by lid lag, upper eyelid retraction, conjunctivitis, redness, among others. In their study, the authors measured the temperature at different regions, including lateral orbit (reference point), cornea, medial and lateral conjunctiva, upper and lower eyelids, and caruncle. They observed significantly higher temperature differences between reference point and other eye regions for the patients suffering from this inflammatory disorder [50].

1.3.1.4 Wound Assessment

A chronic wound is commonly defined as a wound whose healing process is hampered. Commonly, wounds are classified as chronic if they need more than 3 months to heal, i.e., to recover anatomic and functional integrity. Indeed, they may require several years to heal, and in some cases remain unhealed for decades. Patients with this problem can experience pain, reduced mobility, physical and emotional distress as well as social isolation. The Wound Healing Society classifies chronic wounds into four categories: diabetic ulcers, pressure ulcers, venous ulcers, and arterial insufficiency ulcers [51].

In the USA, chronic wounds affect approximately 6.5 million patients (∼2% of the US population) leading to annual costs of about 25 billion US dollars. In the Scandinavian countries, the associated medical costs correspond to 2–4% of the total health care expenses. However, the medical expenditures are increasing rapidly due to aged population and a sharp grow in the incidence of diabetes and obesity worldwide [51].

Thermal imaging can be used for non-invasive assessment of wound severity. The potential of IRT to aid in the assessment of wounds was identified by Lawson in the early 1960s [52]. He used this technology to predict burn depth. Histological analysis confirmed an accuracy of 90%. The author stated that whereas superficial burns are warmer than uninjured skin due to increased inflammatory processes, deeper burns are cooler than uninjured skin owing to structural damage of the vasculature [52]. In 1996, Hansen et al. [53] published a very interesting work where they studied the capability of IRT to assess wound severity of newly formed